Article

Cell Reports

Cell-Autonomous Ca^{2+} Flashes Elicit Pulsed Contractions of an Apical Actin Network to Drive Apical Constriction during Neural Tube Closure

Graphical Abstract

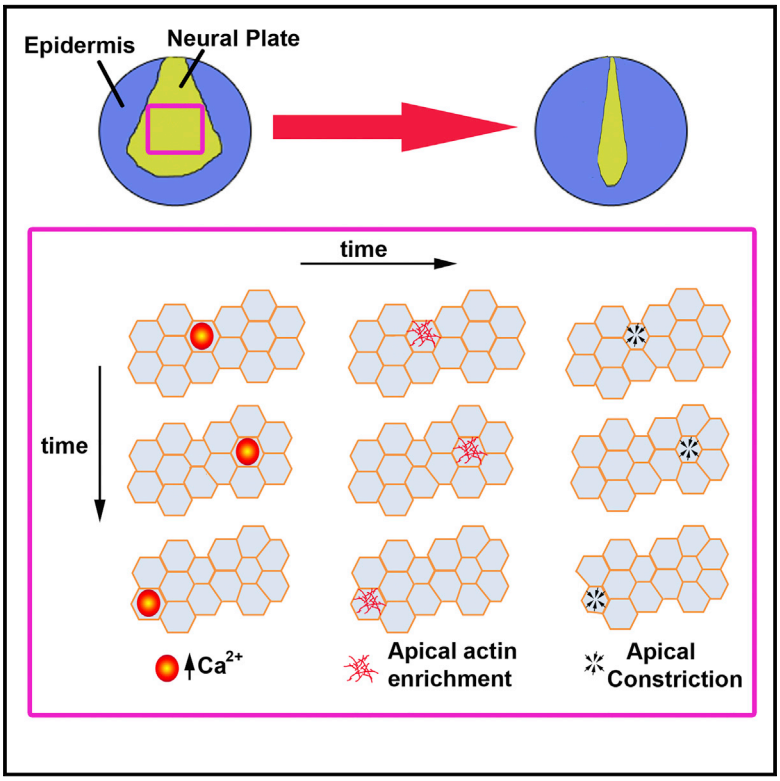

Authors

Neophytos Christodoulou, Paris A. Skourides

Correspondence

skourip@ucy.ac.cy

In Brief

Christodoulou and Skourides show that apical constriction (AC) during neural tube closure (NTC) is a stepwise process driven by cell-autonomous and asynchronous contraction pulses of apical actin. These pulses are elicited by cell-autonomous and asynchronous calcium transients, and the autonomy and asynchrony of contraction are necessary for proper morphogenesis.

Highlights

- Cell-autonomous and asynchronous contractions of apical actin drive AC during NTC
- Cell-autonomous and asynchronous Ca^{2+} flashes precede contraction events during AC
- The autonomy and asynchrony of contraction are necessary for proper morphogenesis
- The Ca^{2+}-dependent protease Calpain2 is a regulator of AC

Christodoulou & Skourides, 2015, Cell Reports *13*, 2189–2202
December 15, 2015 ©2015 The Authors
http://dx.doi.org/10.1016/j.celrep.2015.11.017

Cell Reports
Article

Cell-Autonomous Ca^{2+} Flashes Elicit Pulsed Contractions of an Apical Actin Network to Drive Apical Constriction during Neural Tube Closure

Neophytos Christodoulou[1] and Paris A. Skourides[1,*]
[1]Department of Biological Sciences, University of Cyprus, P.O. Box 20537, 2109 Nicosia, Cyprus
*Correspondence: skourip@ucy.ac.cy
http://dx.doi.org/10.1016/j.celrep.2015.11.017

SUMMARY

Neurulation is a critical period in all vertebrates and results in the formation of the neural tube, which gives rise to the CNS. Apical constriction is one of the fundamental morphogenetic movements that drives neural tube closure. Using live imaging, we show that apical constriction during the neurulation is a stepwise process driven by cell-autonomous and asynchronous contraction pulses followed by stabilization steps. Our data suggest that contraction events are triggered by cell-autonomous Ca^{2+} flashes and are driven by a transient contractile apical pool of actin. In addition, we provide evidence that the cell autonomy and asynchrony of contraction are required for the correct spatial distribution of constriction and, as a result, are critical for tissue morphogenesis. Finally, we identify Calpain2 as a regulator of apical constriction and show that it is required for the stabilization step, but is dispensable during contraction.

INTRODUCTION

During embryogenesis, the coordination of several morphogenetic movements is necessary for the generation of the embryonic architecture. Apical constriction (AC) is a fundamental morphogenetic movement driving cell shape changes during embryogenesis, generating forces for the bending of tissues, the formation of tubes, cell invagination, and wound healing (Martin and Goldstein, 2014). Defects in AC lead to anterior neural tube defects (NTDs) and improper formation of several organs (Haigo et al., 2003). During AC the apical surface of a cell shrinks and is often accompanied by apicobasal cell elongation (Martin and Goldstein, 2014). Contraction of actin filaments by the motor protein myosin is a conserved mechanism driving AC in different organisms. Although the machinery driving AC is conserved in different organisms and tissues, current knowledge suggests that its organization varies among different organisms and tissues (Martin and Goldstein, 2014). Specifically, in vivo studies in invertebrates have shown that apical cell surface shrinkage is driven by pulsed contractions of a medioapical actomyosin network (Martin et al., 2009; Solon et al., 2009), while the predominant model for AC in vertebrates, which is supported by electron microscopy (EM) data, suggests that a circumferential actomyosin network drives apical surface shrinkage according to a purse-string model (Burnside, 1971; Schroeder, 1970).

Ca^{2+} has been implicated in embryogenesis either in the form of Ca^{2+} waves or through Wnt/Ca^{2+} signaling (Kühl et al., 2000a, 2000b; Slusarski et al., 1997a, 1997b). Treatment of vertebrate embryos with pharmacological inhibitors of Ca^{2+} results in defective neural fold formation and neural tube closure (NTC), suggesting a role of Ca^{2+} signaling in AC (Smedley and Stanistreet, 1986). In addition, two recent studies in *Drosophila* provide further evidence of a link between AC and cytosolic Ca^{2+} levels. In the first study it was shown that AC in response to wounding is associated with elevated Ca^{2+} levels (Antunes et al., 2013), and the second study found that, during dorsal closure, Ca^{2+} signaling promotes contractility (Hunter et al., 2014).

Among the numerous molecules that are activated upon Ca^{2+} binding are the Calpain family proteases. Calpains are a family of Ca^{2+}-dependent intracellular cystein proteases that regulate several physiological processes by limited cleavage of different substrates (Wells et al., 2005). We have reported recently that impaired Calpain2 (CAPN2) activity results in defective convergent extension of both mesodermal and neural tissues (Zanardelli et al., 2013).

Here, we show that AC in *Xenopus* is driven by cell-autonomous and asynchronous pulsed contractions, which are followed by stabilization steps. Imaging of actin dynamics demonstrates that contraction pulses are driven by the contraction of a transient apical actin network. We also show that these pulsed contraction events are elicited by cell-autonomous and asynchronous Ca^{2+} flashes, which are an integral part of AC. Pharmacological elevation of cytosolic Ca^{2+} levels leads to synchronous and continuous AC resulting in the failure of NTC, suggesting that asynchronous pulsed contractions are essential for the correct spatial regulation of tissue contraction that shapes tissues and organs. Finally, we identify CAPN2 as a regulator of AC and we demonstrate that, although CAPN2 activity is dispensable for the contraction pulse, it is essential for the stabilization step.

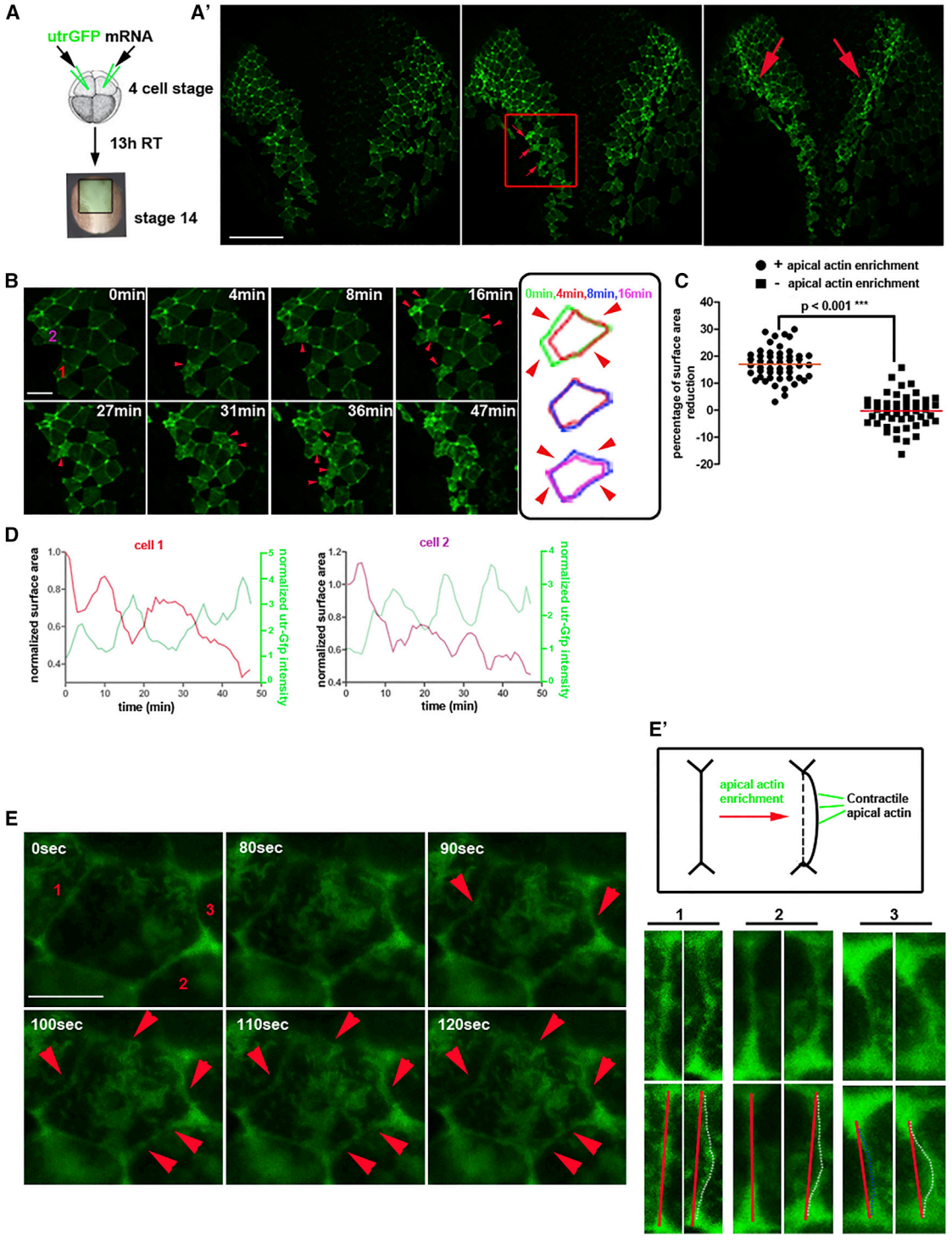

Figure 1. Dynamics of Apical Actin Network during AC of Neuroepithelial Cells

(A) Experimental strategy for imaging actin dynamics during NTC. (A′) Stills from a time-lapse recording (Movie S1) show actin dynamics during NTC. Red arrows indicate cells displaying apical actin enrichment. Scale bar, 100 μm.

(B) Close up of region bound by red box in (A′). Schematic shows the boundaries of an individual cell at different time points. Apical cell surface is reduced after apical actin enrichment events. Scale bar, 20 μm.

(C) Cell surface area changes over a period of 1 min in the absence and presence of apical actin enrichment.

(legend continued on next page)

RESULTS

Pulsed Contractions of an Actin Network Drive AC in the Vertebrate Neural Tube

AC of neuroepithelial cells contributes to the bending and fusion of neural folds during NTC. Several studies have shown that regulators or members of the actomyosin complex are necessary for proper AC of neuroepithelial cells in vertebrates, and defects of the actomyosin complex result in NTDs (Wallingford, 2005). Live imaging in *Drosophila* revealed that AC in invertebrates is driven by contractions of a medioapical actomyosin complex in a ratchet-like fashion (Martin et al., 2009). In contrast, data from EM studies suggest that in vertebrates a circumferential actomyosin complex drives AC (Martin and Goldstein, 2014). However, the model in vertebrates has been inferred from static images, and, to our knowledge, the dynamics of the actomyosin complex during AC in the neural plate have not been documented live in any vertebrate system. We therefore decided to record the actin dynamics of neuroepithelial cells during NTC in *Xenopus*.

To do this, we injected Utrophin-GFP mRNA at the two dorsal blastomeres of four-cell-stage embryos to target the neural plate, allowed them to develop to stage 14, and subsequently imaged the neural plate (Figure 1A). During NTC we observed the transient appearance of a highly dynamic apical actin pool in neuroepithelial cells (Figures 1A and 1B; Movie S1). Apical actin enrichment occurred cell autonomously in the majority of cells (84%, n = 150) and occasionally in small (2–5) or large (>5) groups of cells (16%, n = 150) (Figure S1A; Movie S1). Simultaneous tracking of the cell surface area, using cortical actin as a marker of cell-cell boundaries (adherens junctions coincide with cortical actin in cells of the neural plate, Figure S1B) revealed that apical actin enrichment takes place just before cells begin to constrict (Figure 1B), leading to a 16.96% ± 0.84% (mean ± SEM, n = 50) reduction of the apical cell surface within 1 min from the appearance of apical actin enrichment (Figure 1C). Quantification of the apical cell surface area and apical Utr-GFP intensity over time also revealed that AC during NTC occurs in a stepwise fashion, where the surface area of individual cells is initially reduced (contraction pulse), followed by a slight increase and stabilization (stabilization step) (Figure 1D; Figure S1C).

Tracking contraction events from time-lapse recordings showed that these events are both cell autonomous and asynchronous, similar to the actin enrichment events (Figure S1D; Movie S2). In addition, maximal contraction was always observed during the maxima of apical actin intensity, suggesting a cause-and-effect relationship and leading to the conclusion that AC in vertebrates is likely driven by contractions of apical actin similar to what has been described in invertebrates (Figure 1D; Movie S3). If this apical actin network is in fact contractile and responsible for the contraction pulses, it would be expected to exert forces on cell-cell junctions leading to their displacement (Lang et al., 2014). Indeed, the appearance of the apical actin network was concomitant with apical junction displacement, providing additional evidence that this is a contractile network driving the contraction pulses (Figures 1E and 1E′). Importantly, as shown apical junction displacement is not synchronous but can be temporally resolved within individual cells. Junctions are displaced at different time points during the contraction pulse, something that would not be expected if an apical contractile actin ring was responsible for the contraction. Overall these data show that AC during NTC occurs through discrete cell-autonomous and asynchronous contraction pulses, which are driven by transient apical actin polymerization events.

Mediolateral Junction Shrinkage Contributes to Apical Cell Surface Area Reduction during NTC

As shown during NTC, a subset of cells is actively undergoing surface area reduction driven by apical actin contraction (Movie S1). Quantification of the surface areas of small regions within the neural plate that do not display contraction pulses during the recorded period revealed that the surface areas of such regions also were reduced over time (~5% in 10 min). We then asked, how is this reduction accomplished in the absence of detectable contraction pulses?

Further analysis of such recordings showed that the mediolateral (M/L) cell junctions of ~30% of cells within a representative region shrink over time (Figure 2A), in agreement with a previous study (Nishimura et al., 2012). This is a clearly polar event, and quantification of M/L and anteroposterior (A/P) junction lengths from representative cells indicated that M/L junction length was reduced over time while A/P junction length was constant with slight fluctuations (Figure 2B). Quantification of the apical cell surface area from individual cells showed that M/L junction shrinkage coincided with cell surface area reduction, as expected (Figure 2B). M/L junction length was reduced 27.46% ± 1.95% (mean ± SEM, n = 38) in a period of 10 min, while A/P junction length showed a −0.58% ± 1.77% reduction (mean ± SEM, n = 35) over the same time (Figure 2C). M/L junction shrinkage led to a 14.59% ± 2% reduction of the apical cell surface area over a period of 10 min (mean ± SEM, n = 19) (Figure 2C). These results suggest that surface area reduction in the absence of apical actin-driven AC is stemming from M/L junction shrinkage. Both M/L junction shrinkage and cell-autonomous and asynchronous contraction pulses occur simultaneously during NTC, both contributing to the overall reduction of apical cell surface area in the neural plate (Figure 2D; Movie S4).

Cell-Autonomous and Asynchronous Ca^{2+} Flashes during NTC

As shown, both the assembly of the apical actin network and AC in the neural plate are pulsed. Similar pulsed contractions have

(D) Normalized apical cell surface area and apical utr-GFP intensity over time of cell (two representative cells are shown). See also Movie S3. AC occurs in a stepwise fashion initiated by contraction pulses (reduction of surface area) and followed by stabilization steps. Increase of apical utr-GFP intensity also is pulsed and coincides with contraction pulses.

(E) High-resolution stills from a time-lapse sequence showing a cell with apical actin enrichment. Cell-cell boundaries are initially straight and are gradually displaced inward at different time points (red arrowheads). Scale bar, 10 μm. (E′) Apical actin exerts forces on apical cell junctions, driving their displacement. High-magnification images of cell-cell junctions 1–3 from (E) at 0 s (left) and 120 s (right) are shown.

See also Figure S1.

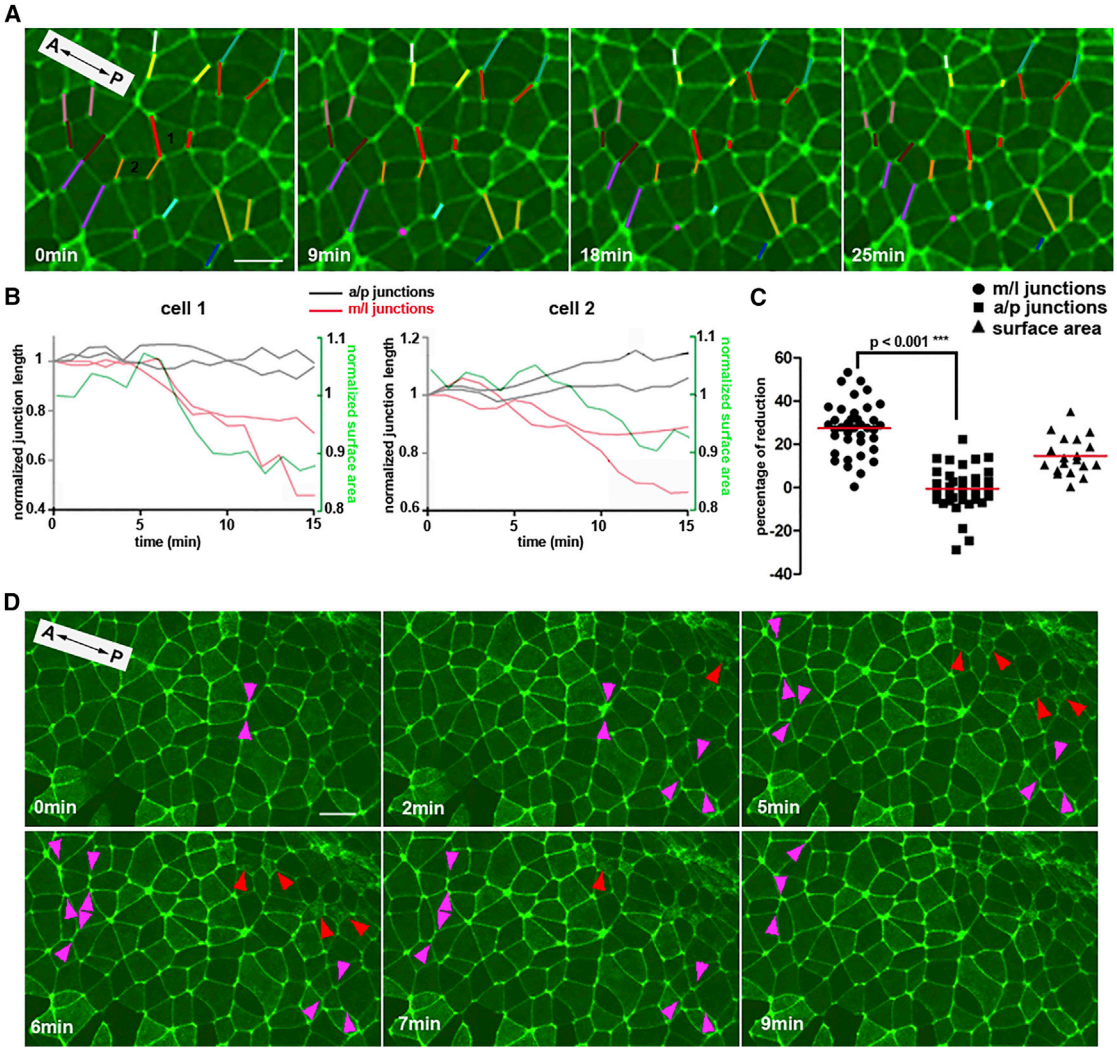

Figure 2. Two Distinct Processes Contribute to Apical Surface Reduction during NTC

(A) Stills from a time-lapse sequence of a representative region within the neural plate of an embryo expressing utr-GFP. Several junctions (color coded) oriented parallel to the M/L axis of the neural plate shrink over time.

(B) Normalized junction length and normalized surface area of indicated cells from (A) over time. M/L junction length (red lines) is reduced over time, while A/P junction length (black lines) remains constant (cell 1) or displays a slight increase (cell 2). Surface area reduction (green line) coincides with shrinking of M/L junctions.

(C) Quantification of M/L junction, A/P junction, and apical cell surface reduction over a 10-min period are shown.

(D) Stills from a time-lapse sequence (Movie S4) of a representative region within the neural plate of an embryo expressing utr-GFP. Purple arrowheads indicate M/L junction shrinkage events. Red arrowheads indicate AC events driven by the enrichment of an apical actin network. Scale bars, 20 μm.

been documented during AC in invertebrates; however, how this pulsed contraction of actomyosin is triggered or regulated is not well understood. The role of Ca^{2+} in muscle contraction is well documented (Szent-Györgyi, 1987), and studies using pharmacological inhibitors have previously implicated Ca^{2+} signaling in NT morphogenesis (Smedley and Stanisstreet, 1986). Furthermore, elevation of intracellular Ca^{2+} has been linked with AC during wound healing and *Drosophila* development (Antunes et al., 2013; Hunter et al., 2014).

We thus decided to image Ca^{2+} levels during NTC using GECO-RED, a genetically coded Ca^{2+} indicator (Zhao et al., 2011). The two dorsal blastomeres of four-cell-stage embryos were injected with mRNAs encoding membrane-GFP and GECO-RED (Figure 3A). Subsequently, embryos were allowed to develop to stage 14 and imaged during NTC (Figure 3A). Live imaging revealed that, despite the lack of frequent Ca^{2+} waves during this process, individual cells in the neural plate frequently displayed rapid transient Ca^{2+} level increases (Figure 3B; Movie S5). The majority of these Ca^{2+} flashes were cell autonomous and asynchronous (Figures 3C and 3D), similar to the contraction pulses and apical actin enrichment events described above. Synchronized Ca^{2+} flashes also were present but occurred with lower frequency in two to five neighboring cells or in larger groups of cells (Figures 3C and 3D). Ca^{2+} flashes were

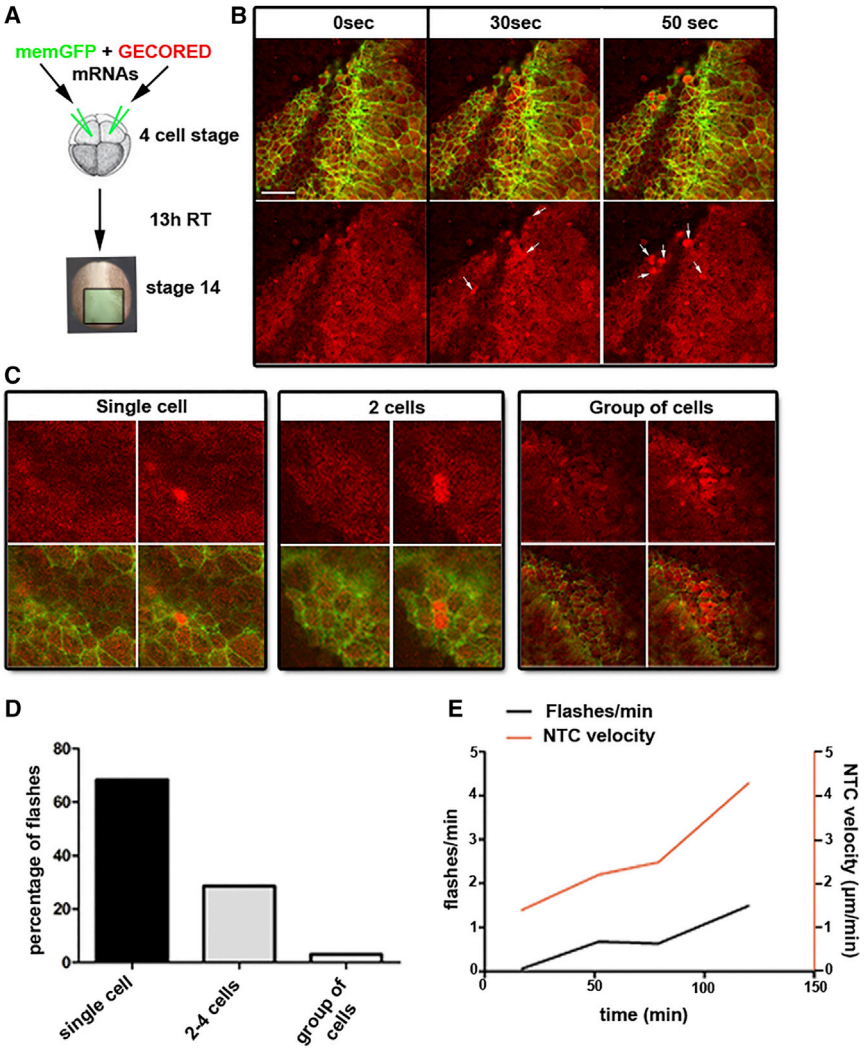

Figure 3. Cell-Autonomous Ca^{2+} Flashes Take Place during Neurulation and Their Frequency Correlates with the Speed of NTC

(A) Experimental strategy for imaging Ca^{2+} dynamics during NTC is shown.

(B) Stills from a time-lapse recording (Movie S5) of anterior NTC from an embryo expressing mem-GFP (green) and GECO-RED (red). Arrows show Ca^{2+} flashes at different time points. Scale bar, 50 μm.

(C) Examples of single-cell, two-cell, and multiple-cell Ca^{2+} flashes are shown.

(D) Quantification shows number of Ca^{2+} flashes occurring in single cells, small group of cells (2–4), or in larger groups of cells (n = 150 events from three embryos).

(E) Graph shows Ca^{2+} flash frequency and NTC speed over time from a representative embryo.

restricted to the neuroepithelium and their frequency was higher in regions like the neural folds, where cells displayed the highest apical cell surface area reduction. Specifically, Ca^{2+} flash frequency of cells near or at the neural folds was 0.25 ± 0.01/min (mean ± SEM, n = 40 cells from three embryos), while the frequency in cells away from the neural folds was about half at 0.11 ± 0.006/min (mean ± SEM, n = 40 cells from three embryos). The typical Ca^{2+} flash was short lived (26 ± 3 s, n = 80 events, three embryos) unlike Ca^{2+} waves reported to take place during mesoderm-convergent extension, which are on the order of minutes (Wallingford et al., 2001). Ca^{2+} flashes increased gradually as NTC progressed, becoming extremely frequent during late stages of NTC; their frequency correlated well with the closure velocity of the NT, suggesting a role in AC (Figure 3E).

Cell-Autonomous and Asynchronous Ca^{2+} Transients Precede Contraction Pulses and Apical Actin Accumulation during NTC

The fact that the majority of Ca^{2+} flashes are cell autonomous and asynchronous, similar to apical actin-driven contraction pulses, and correlate well with the speed of NTC suggests that these transients may have a direct role in AC. However, Ca^{2+} transients also may be secondary events to constriction. To distinguish between these two possibilities, we simultaneously tracked cell cortices (mem-GFP) and Ca^{2+} levels (GECO-RED) of neuroepithelial cells. In all cases, Ca^{2+} flashes preceded the initiation of apical cell surface reduction, showing that Ca^{2+} flashes were not elicited by cell contraction but likely were triggering these events (Figure 4A; Movie S5). Tracking the apical cell surface over a period of 1 min, after a Ca^{2+} flash and without a Ca^{2+} flash, revealed that the mean apical cell surface reduction after a Ca^{2+} flash was 16.41% ± 1.22% (mean ± SEM, n = 65 cells, three embryos), while the mean apical cell surface reduction without a flash was −0.41% ± 0.67% (mean ± SEM, n = 65 cells, three embryos) (Figure 4B). Simultaneous tracking of the cell surface area and Ca^{2+} levels in cells undergoing consecutive contraction pulses demonstrated that Ca^{2+} flashes occurred just before the contraction pulse, but never during the stabilization step, for all cells examined (100%, n = 30 cells, three embryos) (Figures 4C and 4D; Movie S6).

These data suggest that contraction pulses during NTC are triggered by transient Ca^{2+} elevation. Ectopic expression of a number of molecules, including Lulu, has been shown to be sufficient to induce AC ectopically in epithelial cells (Chu et al., 2013; Haigo et al., 2003; Itoh et al., 2014). We thus asked if ectopic induction of AC would elicit ectopic Ca^{2+} flashes in non-neural tissues. Monitoring intracellular Ca^{2+} levels during Lulu-induced AC in gastrula-stage embryos revealed that cell-autonomous Ca^{2+} flashes were in fact generated ectopically in actively constricting cells expressing Lulu-GFP, but not in neighboring control cells. This was true for 97.5% of monitored cells (n = 40) (Figure 4E; Movie S7). Similar to what was observed during

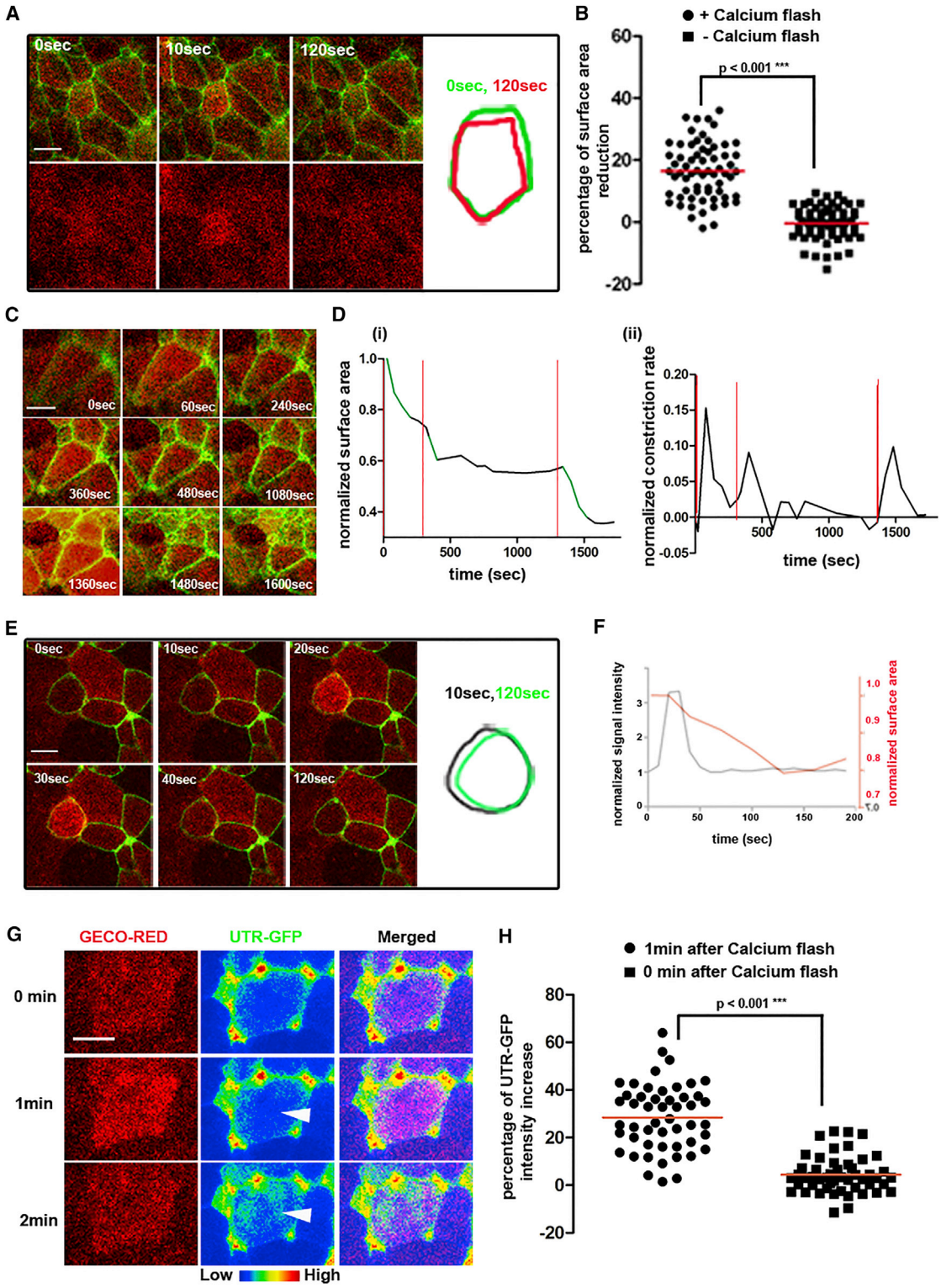

Figure 4. Ca^{2+} Flashes Precede Contraction Pulses

(A) Stills from a time-lapse recording of a region within the neural plate of an embryo expressing GECO-RED (red) and mem-GFP (geen). Cell cortices at 0 s (green) and 120 s (red) are shown.

(B) Apical cell surface reduction of neuroepithelial cells that display a Ca^{2+} flash and ones that do not over a period of 1 min is shown (n = 65 cells, four embryos).

(legend continued on next page)

NTC, ectopic Ca^{2+} flashes induced by Lulu expression always preceded the contraction pulse (100%, n = 39) (Figure 4F). These data suggest that Ca^{2+} flashes are an integral part of AC independent of tissue context.

We went on to examine the temporal relationship between the Ca^{2+} flashes and apical actin enrichment events. Live imaging of NTC in embryos co-expressing GECO-RED and UTR-GFP revealed that apical actin enrichment occurred within 1 min after a Ca^{2+} flash and never occurred before or during a Ca^{2+} flash (Figures 4G and 4H; Movie S8). In addition, no contraction pulses or apical actin enrichment events were detected in the absence of Ca^{2+} flashes. This was true for all neuroepithelial cells examined (n = 50). Overall these data suggest that Ca^{2+} transients are responsible for the pulsed contraction events observed during AC by triggering the formation of a contractile apical actin network.

Cell Autonomy and Asynchrony of Ca^{2+} Flashes Are Necessary for Proper Morphogenesis

The majority of Ca^{2+} transients during NTC occur in a cell-autonomous and asynchronous fashion, leading to asynchronous and cell-autonomous pulsed contractions rather than continuous synchronized contraction. We thus decided to examine the role of this asynchrony and cell autonomy in the process of AC. In an effort to address this, we took advantage of Thapsigargin (THA), an inhibitor of the sarco/endoplasmic reticulum Ca^{2+} ATPase. Use of THA leads to the depletion of Ca^{2+} stores and an overall increase of cytosolic Ca^{2+} levels through the opening of store-operated channels (Dakin et al., 2005). This would presumably lead to Ca^{2+} levels that would be permissive for AC but prevent cell-autonomous Ca^{2+} transients due to the depletion of stores. In addition, THA, unlike Ca^{2+} chelation approaches, would not affect adherens junctions and other Ca^{2+}-dependent components of the cell machinery required for AC.

As predicted, THA treatment led to an increase of baseline cytosolic Ca^{2+} levels in the outer epithelium of the embryo (100%, n = 5 embryos) (Figure 5A). Imaging of Lulu-induced AC in the presence of THA revealed increased overall constriction (100%, n = 5 embryos) (Figure 5B; Movie S9). Lulu-expressing cells underwent AC in the absence of Ca^{2+} flashes in the presence of THA (Movie S10), showing that cell-autonomous Ca^{2+} flashes are not a prerequisite for AC. Quantification of the cell surface area over time from control and THA-treated gastrula embryos revealed that, in treated embryos, ectodermal cells underwent AC via continuous and synchronized contraction (Figure 5C). This was true for 95% of ectodermals cells examined (n = 40 cells, five embryos). These data overall suggest that cytosolic Ca^{2+} levels are linked with the rate of constriction and that the pulsed asynchrony displayed by cells undergoing AC is stemming from the asynchronous and cell-autonomous Ca^{2+} transients. However, it is clear that the cell autonomy and asynchrony of Ca^{2+} transients are not necessary for AC, since overall constriction increased in THA-treated embryos. What then is the purpose of the asynchrony and cell autonomy of contraction if faster constriction can be achieved via continuous and synchronized contraction?

To address this question, we treated neurula-stage embryos with THA. Treated embryos displayed severe NTC defects (100%, n = 20 embryos) (Figure 5D). Imaging of the neural plates of control and treated embryos (n = 20 embryos) revealed that, despite a similar average constriction index (Figure 5E), in treated embryos the spatial distribution of the degree of constriction was disrupted. In control embryos, when the degree of constriction was plotted along the left-to-right axis of the embryo, three areas of increased constriction became evident: two at the lateral hinge points and one at the medial groove. In the presence of THA, this constriction patterning was disrupted and elevated constriction foci became random, as shown in the graph (Figure 5F). These results suggest that asynchronous and cell-autonomous contraction pulses are necessary for the correct temporal and spatial distribution of constriction and, as a result, correct morphogenesis of the NT.

Given the importance of cell-autonomous Ca^{2+} transients for proper constriction patterning, we then asked how these cell-autonomous events are possible given the presence of gap junctions, the specialized low-resistance intercellular channels responsible for the propagation of tissue-level Ca^{2+} waves (Leybaert and Sanderson, 2012). One possibility is that the gap junctions close transiently to allow cell-autonomous intracellular Ca^{2+} flashes by preventing their propagation to neighboring cells. If this explanation is in fact correct, apically constricting cells would presumably fail to respond to tissue-level Ca^{2+} waves. To examine this possibility, we imaged gastrula embryos and monitored Ca^{2+} wave propagation in cells undergoing Lulu-induced AC and neighboring control cells. GECO-RED mRNA was injected in both blastomeres of two-cell-stage embryos and Lulu-GFP mRNA in one blastomere once the embryos reached the four-cell stage and subsequently imaged at gastrula stage. In the provided time-lapse recording (Movie S11), several Lulu-positive cells are visible (red membrane staining) primarily at the right area of the frame. During the first few frames, a number of cell-autonomous Ca^{2+} flashes took place in Lulu-positive cells, and, toward the end of the recording, a strong tissue-level Ca^{2+} wave began to propagate along the ectoderm (Movie S11). From the recording, wave propagation appears to be limited to the Lulu-negative regions

(C) Stills from a time-lapse recording (Movie S6) showing a representative neuroepithelial cell expressing GECO-RED (red) + mem-GFP (green). During the recording this cell displays three Ca^{2+} flashes.
(D) Graph showing the apical cell surface area (i) and constriction rate (ii) with simultaneous tracking of the Ca^{2+} flashes (red lines) of the cell in (C) over time. Ca^{2+} flashes precede the contraction pulses.
(E) Stills from a time-lapse recording (see also Movie S7) show a representative ectodermal cell of a stage-9 embryo expressing Lulu-GFP (green) + GECO RED (red).
(F) Quantification of GECO-RED signal intensity over time (black line) with cell surface area over time (red line). Ca^{2+} flash precedes surface area reduction. Scale bars, 10 μm.
(G) Stills from a time-lapse recording (Movie S8) show a region within the neural plate of an embryo expressing GECO-RED (red) and UTR-GFP (rainbow).
(H) UTR-GFP intensity in neuroepithelial cells 1 min after and during a Ca^{2+} flash is shown (n = 50 events, three embryos). Scale bars, 20 μm.

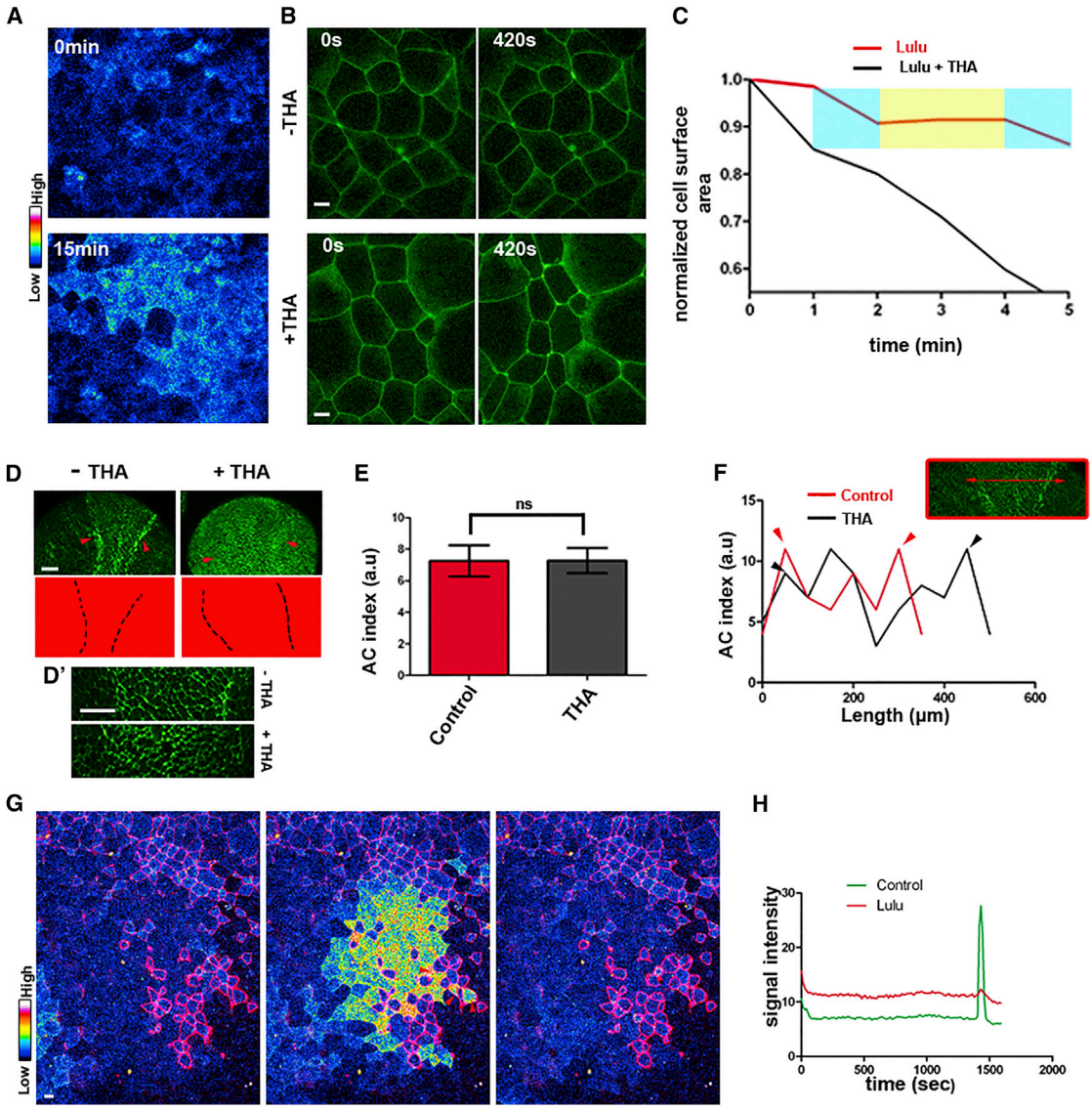

Figure 5. The Asynchrony and the Autonomy of Contraction Are Necessary for NT Morphogenesis

(A) Intensity-coded images of a GECO-RED-expressing gastrula embryo treated with THA. THA treatment results in the gradual increase of intracellular Ca^{2+}.

(B) Stills from time-lapse recordings (Movie S9) of gastrula embryos expressing Lulu-GFP with and without THA. Imaging began 15 min after THA treatment. Scale bars, 20 μm.

(C) Cell surface area over time of representative Lulu-expressing cells from control and THA-treated gastrula embryos. Blue highlight denotes constriction pulses and yellow highlight indicates the stabilization step.

(D) Stage-15 control and THA-treated embryos stained with phalloidin. Red arrowheads indicate the hinge points. Dotted lines show the borders of the neural plate. NTC fails after THA treatment. (D′) High-magnification images show neuroepithelial cells from control and THA-treated neurula embryos. Scale bars, 100 μm.

(E) Mean AC index (number of cells within a circle of a 50-μm diameter) within the neural plate of control and THA-treated embryos is shown (n = 20 regions from five different embryos; mean ± SEM).

(F) Graph of the AC index along the left-to-right axis of representative embryos (red line in inset). Arrowheads mark the neural folds.

(G) Stills from a time-lapse recording (Movie S11) show a stage-11.5 embryo expressing Lulu-GFP (purple) + GECO-RED (intensity coded) during the generation of a Ca^{2+} wave. Scale bar, 20 μm.

(H) GECO-RED signal intensity over time including the Ca^{2+} wave in regions expressing LULU-GFP and control regions (mean; n = 30 cells; ***$p < 0.001$). Ca^{2+} wave initiates at 1,430 s.

of the embryo with apically constricting Lulu-positive cells failing to respond even when surrounded by responding control cells. (Figure 5G; Movie S11).

Quantification of the GECO-RED signal intensity in control cells (n = 15) and cells expressing Lulu GFP (n = 15) confirmed that the majority of Lulu expressors failed to respond to the

Ca^{2+} wave (Figure 5H). This shows that constricting cells were not only able to contain Ca^{2+} transients without depolarizing neighboring cells but they were also unable to respond to the Ca^{2+} elevation of their neighbors. In addition, a comparison of the GECO-RED signal intensity between Lulu expressors and controls showed that the basal levels of cytosolic Ca^{2+} were higher in cells expressing Lulu (Figure 5H). Overall these results show that the cell autonomy and asynchrony of contraction are necessary for correct constriction patterning during NTC, and they show that cell autonomy is achieved through the isolation of constricting cells from the surrounding tissue.

The Ca^{2+}-Regulated Cysteine Protease CAPN2 Is Involved in AC

The presence of Ca^{2+} flashes during NTC and their role during AC suggest that Ca^{2+}-regulated proteins might be involved in this process. We have shown previously that, during *Xenopus* neurulation, expression of CAPN2 is elevated in neural tissues (Zanardelli et al., 2013), in agreement with studies in the mouse and zebrafish (Lepage and Bruce, 2008; Raynaud et al., 2008). We also have shown that CAPN2 is involved in NTC, raising the possibility that it is involved in AC (Zanardelli et al., 2013).

To investigate a possible involvement of CAPN2 in AC, we unilaterally injected embryos with a previously characterized CAPN2 morpholino oligonucleotide (MO), allowed them to develop to stage 16, and fixed and stained for β-catenin. As shown, CAPN2 morphant cells failed to undergo AC (Figures 6A and 6A′). To explore if AC inhibition is cell autonomous, we injected 20 ng CAPN2 MO at one dorsal blastomere at the 16-cell stage. Cells positive for fluorescein isothiocyanate (FITC)-CAPN2 MO showed impaired AC (larger cell surface area), while neighboring cells, negative for CAPN2 MO, were apically constricted, suggesting that the phenotype is cell autonomous (Figure 6B). The AC phenotype was rescued by the expression of CAPN2, suggesting the phenotype is specific (Figure S2A). The mean surface area/cell perimeter ratio in morphant cells was higher than in control cells, and it was rescued when the MO was coinjected with CAPN2R mRNA (Figure 6C). In addition, cell height was significantly affected in CAPN2 MO-injected cells, and this phenotype also could be partially rescued (Figure 6D**)**. Treatment of embryos with Calpain Inhibitor III (CI3) induced identical phenotypes (data not shown), providing additional support for the specificity of the phenotype.

To rule out the possibility that the AC defects in CAPN2 morphants were stemming from general defects in apicobasal polarity and/or tight junction assembly, we examined the localization of ZO-1 Par6, αPKC, and cortactin in morphant embryos. As shown, ZO-1 localization was unaffected in morphant neuroepithelial cells despite defective AC (Figures 6E and 6E′). Localization of Par6, αPKC, and cortactin also was unaffected after CAPN2 downregulation (Figures S2B–S2D). These data indicate that CAPN2 downregulation affects AC in neuroepithelial cells without affecting apico-basal polarity. In agreement with the role of CAPN2 in AC, CAPN2 morphant embryos display phenotypes linked with AC. As shown, unilateral downregulation of CAPN2 resulted in failure of neural fold elevation (95% of embryos, n = 80) (Figure 6G). At tailbud stage, the anterior NT failed to close at the MO-injected side, while posterior NTC was delayed but eventually completed (Figures 6G and 6G′). Cytokeratin (epidermal marker) staining of unilaterally MO-injected tailbud embryos revealed that the anterior neural plate at the injected side remained exposed (Figures 6H and 6H′), confirming anterior NTC defects. In addition, at tadpole stages, CAPN2 downregulation in neural tissues resulted in anencephaly (Figure S2E), a phenotype linked to defective rostral NTC (Golden and Chernoff, 1995).

Beyond its role during neurulation, AC has an important role in the formation of several organs (Chung et al., 2010; Lee et al., 2007; Llimargas and Casanova, 2010; Plageman et al., 2011). CAPN2 mRNA is enriched in all tissues undergoing AC in *Xenopus* (Figures S2F–S2H), similar to other regulators of AC (Lee et al., 2009). Loss-of-function experiments revealed that CAPN2 is indispensable for AC during gut, cement gland, and olfactory placode formation, through its involvement in AC (Figures S2I–S2O). These results indicate that CAPN2 is important for AC in a tissue-context-independent manner.

CAPN2 Is Required for the Stabilization Step during AC

CAPN2 also has been implicated in the convergent extension (CE) of mesodermal and neural tissues (Zanardelli et al., 2013). To exclude the possibility that the AC defects elicited by CAPN2 downregulation are indirect due to defects in CE or tissue specification issues, we examined the requirement of CAPN2 function in ectopically induced AC. Injections of Shroom3, Lulu-GFP, or GEF-H1 mRNA at one dorsal blastomere of four-cell-stage embryos induced AC in ectodermal cells expressing these molecules at the gastrula stage (Figures S3A–S3C), as expected (Chu et al., 2013; Haigo et al., 2003; Itoh et al., 2014). As shown, CAPN2 inhibition led to a partial block of constriction in all three cases (Figures S3A–S3C). These results suggest that defective AC of morphant neuroepithelial cells is a direct effect of CAPN2's role in AC.

As described before, AC induced by Lulu-GFP expression was driven by contraction pulses followed by stabilization steps (Figure S3D), in a similar fashion to what we documented in the neural plate. To examine the mechanism behind CAPN2's involvement in AC, we carried out live imaging of Lulu-GFP-expressing ectodermal cells from early gastrula embryos in the presence and absence of CI3. Cells were imaged immediately after cell division was completed to ensure that CI3-treated and control embryos were at the same stage of the cell cycle. Lulu-induced AC was visibly impaired in CI3-treated embryos, as expected (Figure 7A), and quantification of the cell surface area over time from 20 different cells confirmed this (Figure 7B). Imaging Ca^{2+} levels in LuLu-GFP-expressing cells revealed that Ca^{2+} flashes occurred normally in the presence of CI3 (Figure 7C) and triggered contraction pulses (Figure 7C′), just like in control embryos (Figure 4E).

Quantification of the constriction rate from 20 cells confirmed that positive events, representing contraction pulses, were taking place normally in both control and CI3-treated Lulu-expressing cells (Figure 7D). However, cells from CI3-treated embryos, unlike controls, displayed frequent negative events (cell surface area increased after the constriction pulse), suggesting that blockage of CAPN2 function leads to defects in the stabilization step (Figure 7D). To further analyze this defect, we quantified the

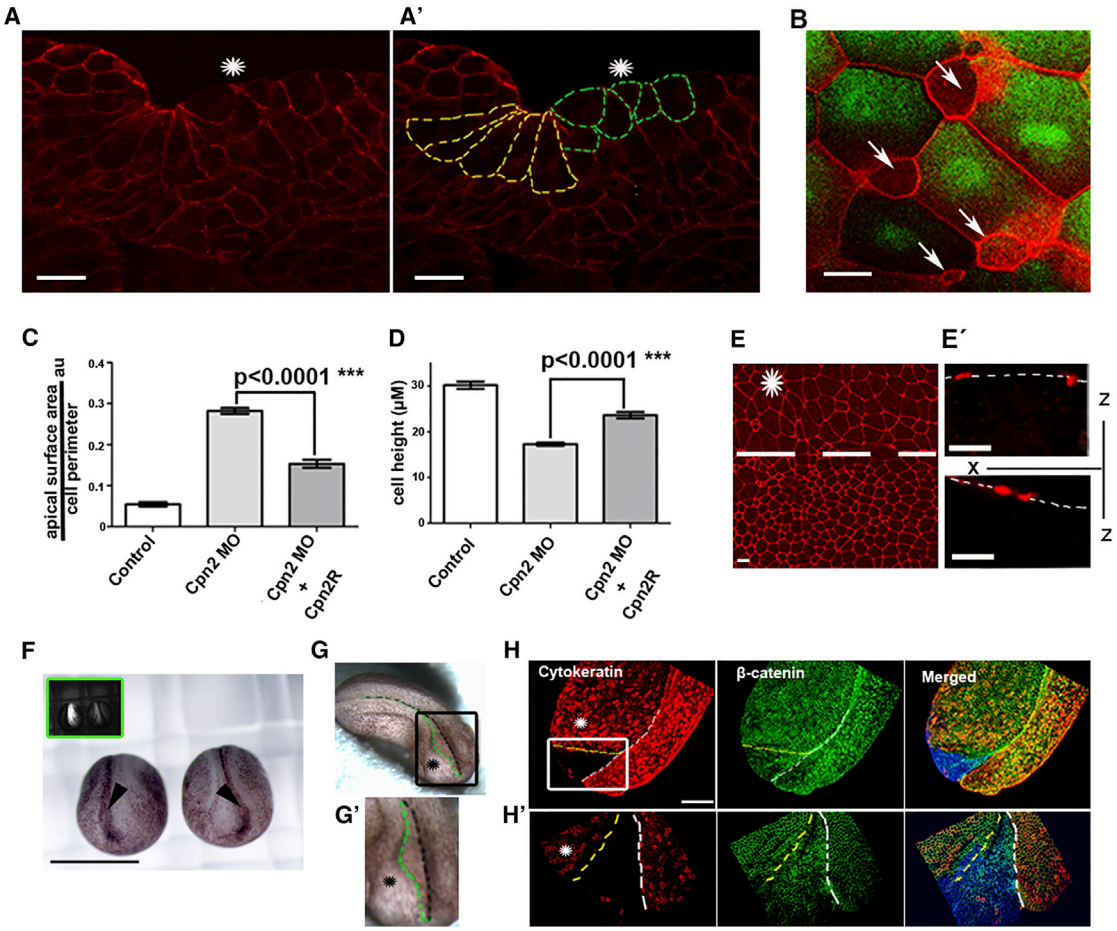

Figure 6. CAPN2 Is Implicated in AC during NTC

(A) Cross-section of a neurula-stage embryo injected at one dorsal blastomere at the four-cell stage with 40 ng CAPN2MO and stained with β-catenin. Injected side is indicated by an asterisk. β-catenin staining was used to trace the cortices of superficial cells (A′). Scale bar, 20 μm.

(B) Dorsal view of neuroepithelial cells stained for β-catenin. GFP indicates CAPN2 morphants. Scale bar, 5 μm.

(C) Mean apical surface area/perimeter ratio of CAPN2MO and CAPN2MO + CAPN2R neuroepithelial cells is shown (n = 40, mean ± SEM).

(D) Mean cell height of control, CAPN2MO, and CAPN2MO + CAPN2R neuroepithelial cells is shown (n = 40, mean ± SEM).

(E) Dorsal view maximum-intensity projection image of the neuroepithelium from an embryo unilaterally injected with 40 ng CAPN2MO and stained for the tight junction marker ZO-1. Injected side is marked (*). Scale bar, 10 μm. (E′) X-Z projections of morphant and control cells are shown. Epithelial cell layer is shown with a dotted line. Scale bar, 5 μm.

(F) Dorsal view of neurula embryos injected with 40 ng CAPN2 MO + 50 pg memGFP RNA at one dorsal blastomere at the four-cell stage. The injected side is GFP positive (inset). Scale bar, 1 mm.

(G) Dorsal view of a tailbud embryo injected with 40 ng CAPN2MO at one dorsal blastomere at the four-cell stage. (G′) Magnification shows the anterior part of the embryo shown in (D). Black lines indicate the midline at the uninjected side and green lines indicate the margins of epidermis at the injected side. Injected side is marked (*).

(H) Dorsal view of tailbud morphant embryo stained with cytokeratin and β-catenin. MO-injected side is GFP positive (blue). White lines mark the midline and green lines mark the margins of the epidermis at the injected side. (H′) Magnified images show the anterior part of the embryo shown in (E). Scale bar, 500 μm. Injected side is marked (*).

pulse magnitude, the number of pulses per minute, and the number of stretching events per minute in control and CI3-treated embryos. This analysis showed that the pulse magnitude was not significantly affected by CAPN2 inhibition (Figure 7E) and that the number of pulses per minute was only slightly reduced (Figure 7F). This indicates that blockage of CAPN2 function leads to mild changes in the frequency of the contraction pulses and has no effect on the magnitude of each contraction. Quantification of the stretching events, however, revealed that the number of stretching events was significantly higher in the presence of CI3 (Figure 7G), confirming that defects in AC are primarily stemming from a requirement of CAPN2 activity during the stabilization step.

DISCUSSION

Neurulation is a critical period in the development of all vertebrate embryos during which the CNS is formed. NTDs are one

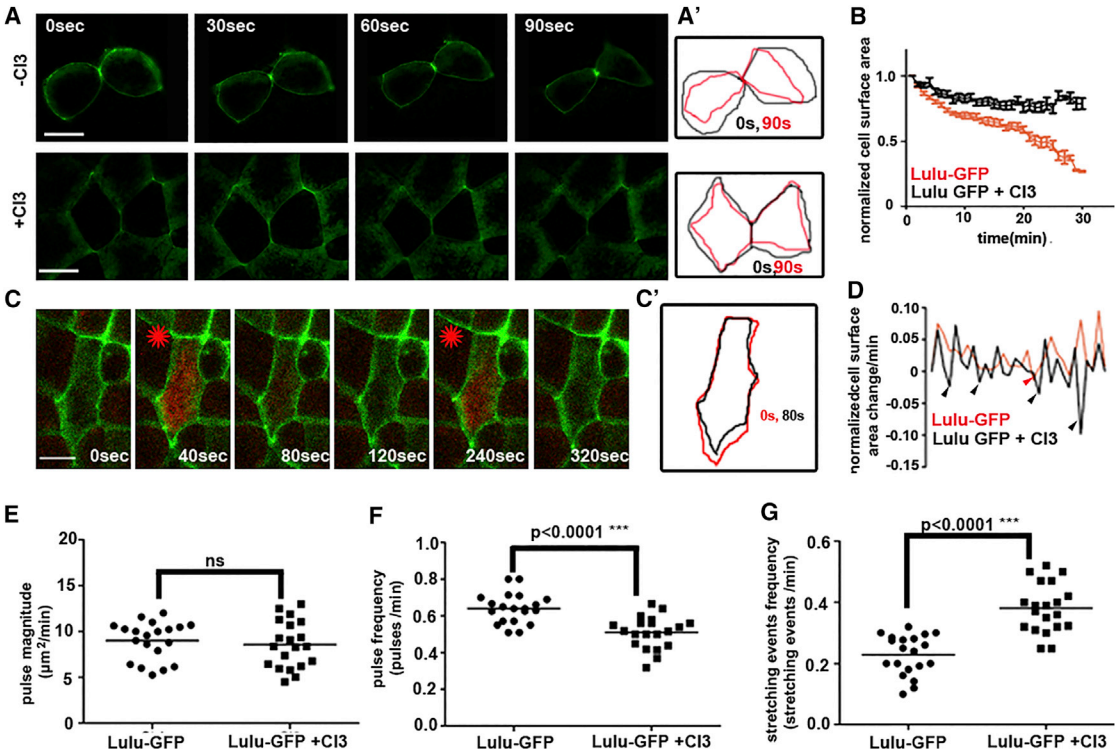

Figure 7. CAPN2 Activity Is Necessary for the Stabilization Step during AC

Effect of CAPN2 inhibition on Lulu-induced AC.

(A) Stills from time-lapse recordings show representative ectodermal cells from gastrula embryos expressing Lulu-GFP with and without CI3. Scale bar, 10 μm.

(A′) Cell cortices at 0 and 90 s are shown.

(B) Graph shows the normalized cell surface area over time with and without CI3 treatment (n = 20; mean ± SEM for each time point).

(C) Stills from a time-lapse recording of a representative cell from gastrula embryo expressing Lulu-GFP (green) + GECO RED (GFP) and treated with CI3. Red stars mark the frames where Ca^{2+} flashes take place Scale bar, 20 μm. (C′) Tracking of the cell cortex shows that, after a Ca^{2+} flash, a contraction pulse takes place.

(D) Graph shows the normalized cell surface area change/minute in control and CI3-treated cells (n = 20 cells from three different embryos; mean for each time point; ***p < 0.001).

(E–G) Graphs show the pulse magnitude (μm^2/min, n = 20) (E), pulse frequency (number of events with apical cell surface area reduction /minute, n = 20) (F), and stretching events frequency (number of events with apical cell surface area increase/minute, n = 20) (G) in control and CI3-treated embryos.

of the most common human birth defects (Copp and Greene, 2010), and, as a result, delineation of the mechanisms driving NTC will lead to a better understanding of human NTDs. In this study, we used live imaging combined with gain- and loss-of-function approaches to explore AC, one of the fundamental morphogenetic movements that drives NTC.

Our work reveals that apical surface reduction of neuroepithelial cells is achieved via two distinct mechanisms: AC through discrete, cell-autonomous contraction events and M/L junction shrinkage. Both processes take place simultaneously during NTC and contribute to the shaping of the tissue (Figures 1 and 2).

M/L junction shrinkage results in polar surface area reduction and it is believed to drive tissue bending toward the midline, helping to close the NT. Previous studies have shown that this process is regulated downstream of the planar cell polarity (PCP) pathway (Nishimura et al., 2012).

The predominant model for AC during NTC prior to this work suggested that contraction of a circumferential actomyosin complex is responsible for the cell shape changes within the neural plate (Burnside, 1971; Schroeder, 1970). This was further supported by data showing that the induction of AC in polarized epithelial cells promotes the formation of circumferential actomyosin complex with sarcomeric organization (Hildebrand, 2005). However, in invertebrate models, several lines of evidence suggest that a contractile pool of apical actin is responsible for AC (Martin and Goldstein, 2014). We now suggest that AC of neuroepithelial cells is similarly driven by transient, cell-autonomous, and asynchronous apical actin enrichment events. In agreement with our data, apical actin contractile filaments previously have been suggested to play a role in vertebrate AC during mouse lens formation (Lang et al., 2014). We show that transient apical actin polymerization events occur during the contraction pulse, and we provide evidence that this actin pool is responsible for the apical surface reduction (Figure 1). First, the appearance of this pool correlates with the initiation of apical surface reduction and maximal reduction occurs when the intensity of the actin pool reaches its maximum. Second, apical actin enrichment correlates with inward apical cell-cell junction displacement that

leads to local bending of the cell-cell boundary. If a circumferential belt of contractile actomyosin was driving AC, it would be expected that such deformations would be synchronized in each cell as the actomyosin ring would contract; however, as we show, these events are not synchronous and can be temporally resolved. This suggests that the apical actin network is responsible for the cell-cell junction displacement that results in apical surface reduction; however, it is also possible that it is a result of the combination of contraction of both the apical actin and of a circumferential actomyosin belt.

Our work suggests that contraction pulses during AC are driven by contraction of an apical actin pool and are elicited by Ca^{2+} flashes. Interestingly, studies using Ca^{2+} chelators have shown that Ca^{2+} is necessary for neural fold formation and NTC in vertebrates (Ferreira and Hilfer, 1993; Smedley and Stanisstreet, 1986). However, these studies could not link Ca^{2+} directly with AC since these experimental approaches also led to defects in Ca^{2+}-dependent cell-cell adhesion. Here we directly link Ca^{2+} levels with AC. We show that cell-autonomous Ca^{2+} flashes are generated during NTC in *Xenopus* and that their frequency correlates with the NTC rate (Figure 3). In addition, we establish that Ca^{2+} flashes occur just before apical cell surface narrowing and apical actin accumulation, suggesting that they trigger the contraction pulses probably by inducing apical actin accumulation (Figure 4). Taken together, these results strongly suggest that Ca^{2+} is a critical regulator of AC.

The mechanism behind the regulation of contraction pulses by Ca^{2+} warrants further study. It has been established that Ca^{2+} influx leads to activation of RhoA during smooth muscle contraction (Sakurada et al., 2003) and endothelial cell spreading (Masiero et al., 1999). Apical accumulation of RhoA is necessary for proper AC and NTC (Kinoshita et al., 2008). RhoA leads to ROCK activation, which has been shown to be necessary for the contraction pulses (Mason et al., 2013). Active ROCK phosphorylates myosin light chain, driving the contraction of actin filaments. Moreover, Ca^{2+} levels also may regulate the actin cytoskeleton directly via Ca^{2+}-regulated actin-binding proteins, such as Gelsolin (Antunes et al., 2013). The very transient nature of these events requires in vivo imaging and the parallel use of FRET sensors to establish how the activation states of molecules like Rho and ROCK are temporally modulated by Ca^{2+} levels.

Of particular interest is the fact that Ca^{2+} flashes and the subsequent apical actin enrichment events are asynchronous and cell autonomous, leading to cell-autonomous and asynchronous contraction pulses. Use of THA leads to elevated Ca^{2+} levels in the tissue, eliminating Ca^{2+} flashes. This leads to synchronized continuous contraction. Despite similar average constriction index in the neural plates of THA-treated embryos compared to controls, THA treatment leads to failure of NTC. Examination of control embryos revealed that, as previously described, three areas of increased constriction are present, two at the left and right hinge points and a third in the medial hinge region (Figure 5). This patterned constriction is lost in THA-treated embryos, with foci of increased constriction found randomly distributed within the neural plate. The above data suggest that cell-autonomous pulses are a prerequisite in order to properly orchestrate the spatial and temporal distribution of constricting cells as well as the extent to which they constrict. In the absence of this regulation, the tissue does not bend at the right places at the right time and/or to the correct extent to achieve NTC. Support for this interpretation comes from recent work in *Drosophila*. Constitutive activation of myosin during *Drosophila* ventral furrow formation also was shown to promote continuous rather than pulsed AC. Although loss of pulsed constriction did not affect the mean constriction rate, it led to delays of invagination, again suggesting that pulsed constriction is required for correct tissue morphogenesis (Vasquez et al., 2014).

Given the importance of cell-autonomous contractions during AC, we then asked, how is this autonomy accomplished? Ca^{2+} waves primarily are propagated through gap junctions (Oshima, 2014). We showed that Ca^{2+} flashes in constricting cells are not propagated to neighboring control cells and that tissue-level Ca^{2+} waves are propagated by control cells but fail to elicit responses from constricting cells (Figure 5). These results suggest that actively constricting cells are effectively isolated from their neighbors likely via closure of their gap junctions. The mechanism behind this isolation of cells undergoing AC is unclear; however, gap junctions have been shown to be regulated by Ca^{2+} levels and close when intracellular Ca^{2+} levels are raised (Oshima, 2014). Our data suggest that constricting cells maintain elevated cytosolic Ca^{2+} levels, which may lead to gap junction closure, thus preventing Ca^{2+} transients from spreading.

The importance of cytosolic Ca^{2+} during AC suggests that Ca^{2+}-regulated proteins must be involved in this process. Here we go on to identify CAPN2 as one of these proteins. CAPN2 is a Ca^{2+}-regulated cysteine protease CAPN2 that displays elevated expression in neural and other tissues shaped by AC. CAPN2 downregulation results in rostral NTDs and we now show that these in part stem from defective AC (Figure 6). We go on to show that CAPN2 is not required for the contraction step, but is for the subsequent stabilization (Figure 7). The latter suggests that Ca^{2+}elevation leads not only to the activation of proteins involved in the contraction pulses, but also leads to activation of proteins that are indispensable for the subsequent stabilization step.

EXPERIMENTAL PROCEDURES

Embryo Injections and Manipulations

Female adult *Xenopus laevis* frogs were induced to ovulate by injection of human chorionic gonadotropin. Eggs were fertilized in vitro, dejellied in 2% cysteine (pH 7.8), and subsequently reared in 0.1× Marc's Modified Ringers (MMR) and staged according to Neiuwkoop and Faber (Nieuwkoop and Faber, 1994). Embryos were microinjected as previously described (Zanardelli et al., 2013). Capped mRNA was in vitro transcribed using mMessage machine kits (Ambion). CI3 (100 μM, Millipore) and 2.5 μM THA 0.1× MMR were added to the embryos at different times of development.

DNA Constructs and MO

HA-tagged CAPN2 rescue construct (CAPN2R) was generated as described before (Zanardelli et al., 2013). CAPN2 antisense MO was obtained from Gene Tools (Zanardelli et al., 2013). GECO-RED construct was bought from Addgene and subcloned into CS108 plasmid for in vitro transcription. Shroom3 construct was kindly provided by Dr. Wallingford. Lulu-GFP and GEF-H1 constructs were kindly provided by Dr. Sokol. HA-Par6 construct was kindly provided by Dr. Daar.

Immunofluorescence

Immunofluorescence analysis was carried out as previously described (Zanardelli et al., 2013). The primary antibodies used were as follows: mouse monoclonal anti-Cytokeratin (Hybridoma Bank, 1h5-c), rabbit polyclonal anti-β-catenin (Santa Cruz Biotechnology, H-102), rabbit polyclonal anti-ZO1 (Invitrogen, 402200), and rabbit polyclonal anti-PKCζ (Santa Cruz, F1013). Embryos were incubated with the specific primary antibody for 4 hr at room temperature (RT) or overnight at 4°C. The secondary antibodies used were as follows: anti-mouse and anti-rabbit Alexa-488 (Invitrogen) and anti-rabbit Cy3 (Jackson ImmunoResearch Laboratories).

Imaging Analysis

Bright-field images were captured on a Zeiss LumarV12 fluorescent stereomicroscope. Fluorescent images were captured either under a Zeiss Axio Imager Z1 microscope, using a Zeiss Axiocam MR3 and the Axiovision software 4.8.2, or under a confocal LSM710 microscope (Zeiss), using Zen 2010 software.

Quantifications of AC Index, Contraction Pulses, and Stretching Events

Quantifications were achieved as follows:

AC index: number of cells within a circle of 50-μm diameter
Contraction pulses: $(ACSA_{t-1} - ACSA_t) > 0$, where ACSA is the apical cell surface area
Stretching events: $(ACSA_{t-1} - ACSA_t) < 0$, where ACSA is the apical cell surface area

Statistical Analysis

All data were analyzed with GraphPad Prism 5 software. Statistical analysis was performed using Student's t test.

SUPPLEMENTAL INFORMATION

Supplemental Information includes three figures and eleven movies and can be found with this article online at http://dx.doi.org/10.1016/j.celrep.2015.11.017.

ACKNOWLEDGMENTS

We thank Dr. Sara Zanardelli for her assistance in the design of the initial experiments regarding CAPN2 function. We also thank Drs. John Wallingford, Sergei Sokol, and Ira. O. Daar for kindly providing plasmids. Funding was provided by the Cyprus Research Promotion Foundation (ΠΕΝΕΚ/0311/36) and co-funded by the Structural Funds of the European Union.

Received: May 21, 2015
Revised: September 13, 2015
Accepted: November 3, 2015
Published: December 3, 2015

REFERENCES

Antunes, M., Pereira, T., Cordeiro, J.V., Almeida, L., and Jacinto, A. (2013). Coordinated waves of actomyosin flow and apical cell constriction immediately after wounding. J. Cell Biol. *202*, 365–379.

Burnside, B. (1971). Microtubules and microfilaments in newt neuralation. Dev. Biol. *26*, 416–441.

Chu, C.W., Gerstenzang, E., Ossipova, O., and Sokol, S.Y. (2013). Lulu regulates Shroom-induced apical constriction during neural tube closure. PLoS ONE *8*, e81854.

Chung, M.I., Nascone-Yoder, N.M., Grover, S.A., Drysdale, T.A., and Wallingford, J.B. (2010). Direct activation of Shroom3 transcription by Pitx proteins drives epithelial morphogenesis in the developing gut. Development *137*, 1339–1349.

Copp, A.J., and Greene, N.D. (2010). Genetics and development of neural tube defects. J. Pathol. *220*, 217–230.

Dakin, K., Zhao, Y., and Li, W.H. (2005). LAMP, a new imaging assay of gap junctional communication unveils that Ca2+ influx inhibits cell coupling. Nat. Methods *2*, 55–62.

Ferreira, M.C., and Hilfer, S.R. (1993). Calcium regulation of neural fold formation: visualization of the actin cytoskeleton in living chick embryos. Dev. Biol. *159*, 427–440.

Golden, J.A., and Chernoff, G.F. (1995). Multiple sites of anterior neural tube closure in humans: evidence from anterior neural tube defects (anencephaly). Pediatrics *95*, 506–510.

Haigo, S.L., Hildebrand, J.D., Harland, R.M., and Wallingford, J.B. (2003). Shroom induces apical constriction and is required for hingepoint formation during neural tube closure. Curr. Biol. *13*, 2125–2137.

Hildebrand, J.D. (2005). Shroom regulates epithelial cell shape via the apical positioning of an actomyosin network. J. Cell Sci. *118*, 5191–5203.

Hunter, G.L., Crawford, J.M., Genkins, J.Z., and Kiehart, D.P. (2014). Ion channels contribute to the regulation of cell sheet forces during Drosophila dorsal closure. Development *141*, 325–334.

Itoh, K., Ossipova, O., and Sokol, S.Y. (2014). GEF-H1 functions in apical constriction and cell intercalations and is essential for vertebrate neural tube closure. J. Cell Sci. *127*, 2542–2553.

Kinoshita, N., Sasai, N., Misaki, K., and Yonemura, S. (2008). Apical accumulation of Rho in the neural plate is important for neural plate cell shape change and neural tube formation. Mol. Biol. Cell *19*, 2289–2299.

Kühl, M., Sheldahl, L.C., Malbon, C.C., and Moon, R.T. (2000a). Ca(2+)/calmodulin-dependent protein kinase II is stimulated by Wnt and Frizzled homologs and promotes ventral cell fates in Xenopus. J. Biol. Chem. *275*, 12701–12711.

Kühl, M., Sheldahl, L.C., Park, M., Miller, J.R., and Moon, R.T. (2000b). The Wnt/Ca2+ pathway: a new vertebrate Wnt signaling pathway takes shape. Trends Genet. *16*, 279–283.

Lang, R.A., Herman, K., Reynolds, A.B., Hildebrand, J.D., and Plageman, T.F., Jr. (2014). p120-catenin-dependent junctional recruitment of Shroom3 is required for apical constriction during lens pit morphogenesis. Development *141*, 3177–3187.

Lee, C., Scherr, H.M., and Wallingford, J.B. (2007). Shroom family proteins regulate gamma-tubulin distribution and microtubule architecture during epithelial cell shape change. Development *134*, 1431–1441.

Lee, C., Le, M.P., and Wallingford, J.B. (2009). The shroom family proteins play broad roles in the morphogenesis of thickened epithelial sheets. Dev. Dyn. *238*, 1480–1491.

Lepage, S.E., and Bruce, A.E. (2008). Characterization and comparative expression of zebrafish calpain system genes during early development. Dev. Dyn. *237*, 819–829.

Leybaert, L., and Sanderson, M.J. (2012). Intercellular Ca(2+) waves: mechanisms and function. Physiol. Rev. *92*, 1359–1392.

Llimargas, M., and Casanova, J. (2010). Apical constriction and invagination: a very self-reliant couple. Dev. Biol. *344*, 4–6.

Martin, A.C., and Goldstein, B. (2014). Apical constriction: themes and variations on a cellular mechanism driving morphogenesis. Development *141*, 1987–1998.

Martin, A.C., Kaschube, M., and Wieschaus, E.F. (2009). Pulsed contractions of an actin-myosin network drive apical constriction. Nature *457*, 495–499.

Masiero, L., Lapidos, K.A., Ambudkar, I., and Kohn, E.C. (1999). Regulation of the RhoA pathway in human endothelial cell spreading on type IV collagen: role of calcium influx. J. Cell Sci. *112*, 3205–3213.

Mason, F.M., Tworoger, M., and Martin, A.C. (2013). Apical domain polarization localizes actin-myosin activity to drive ratchet-like apical constriction. Nat. Cell Biol. *15*, 926–936.

Nieuwkoop, P.D., and Faber, J. (1994). Normal Table of Xenopus Laevis (Daudin) (New York: Garland Science).

Nishimura, T., Honda, H., and Takeichi, M. (2012). Planar cell polarity links axes of spatial dynamics in neural-tube closure. Cell *149*, 1084–1097.

Oshima, A. (2014). Structure and closure of connexin gap junction channels. FEBS Lett. *588*, 1230–1237.

Plageman, T.F., Jr., Chauhan, B.K., Yang, C., Jaudon, F., Shang, X., Zheng, Y., Lou, M., Debant, A., Hildebrand, J.D., and Lang, R.A. (2011). A Trio-RhoA-Shroom3 pathway is required for apical constriction and epithelial invagination. Development *138*, 5177–5188.

Raynaud, F., Marcilhac, A., Chebli, K., Benyamin, Y., and Rossel, M. (2008). Calpain 2 expression pattern and sub-cellular localization during mouse embryogenesis. Int. J. Dev. Biol. *52*, 383–388.

Sakurada, S., Takuwa, N., Sugimoto, N., Wang, Y., Seto, M., Sasaki, Y., and Takuwa, Y. (2003). Ca2+-dependent activation of Rho and Rho kinase in membrane depolarization-induced and receptor stimulation-induced vascular smooth muscle contraction. Circ. Res. *93*, 548–556.

Schroeder, T.E. (1970). Neurulation in Xenopus laevis. An analysis and model based upon light and electron microscopy. J. Embryol. Exp. Morphol. *23*, 427–462.

Slusarski, D.C., Corces, V.G., and Moon, R.T. (1997a). Interaction of Wnt and a Frizzled homologue triggers G-protein-linked phosphatidylinositol signalling. Nature *390*, 410–413.

Slusarski, D.C., Yang-Snyder, J., Busa, W.B., and Moon, R.T. (1997b). Modulation of embryonic intracellular Ca2+ signaling by Wnt-5A. Dev. Biol. *182*, 114–120.

Smedley, M.J., and Stanisstreet, M. (1986). Calcium and neurulation in mammalian embryos. II. Effects of cytoskeletal inhibitors and calcium antagonists on the neural folds of rat embryos. J. Embryol. Exp. Morphol. *93*, 167–178.

Solon, J., Kaya-Copur, A., Colombelli, J., and Brunner, D. (2009). Pulsed forces timed by a ratchet-like mechanism drive directed tissue movement during dorsal closure. Cell *137*, 1331–1342.

Szent-Györgyi, A.G. (1987). Muscle contraction: calcium in muscle activation. Science *238*, 223.

Vasquez, C.G., Tworoger, M., and Martin, A.C. (2014). Dynamic myosin phosphorylation regulates contractile pulses and tissue integrity during epithelial morphogenesis. J. Cell Biol. *206*, 435–450.

Wallingford, J.B. (2005). Neural tube closure and neural tube defects: studies in animal models reveal known knowns and known unknowns. Am. J. Med. Genet. C. Semin. Med. Genet. *135C*, 59–68.

Wallingford, J.B., Ewald, A.J., Harland, R.M., and Fraser, S.E. (2001). Calcium signaling during convergent extension in Xenopus. Curr. Biol. *11*, 652–661.

Wells, A., Huttenlocher, A., and Lauffenburger, D.A. (2005). Calpain proteases in cell adhesion and motility. Int. Rev. Cytol. *245*, 1–16.

Zanardelli, S., Christodoulou, N., and Skourides, P.A. (2013). Calpain2 protease: A new member of the Wnt/Ca(2+) pathway modulating convergent extension movements in Xenopus. Dev. Biol. *384*, 83–100.

Zhao, Y., Araki, S., Wu, J., Teramoto, T., Chang, Y.F., Nakano, M., Abdelfattah, A.S., Fujiwara, M., Ishihara, T., Nagai, T., and Campbell, R.E. (2011). An expanded palette of genetically encoded Ca^{2+} indicators. Science *333*, 1888–1891.